PROCEEDINGS OF SPIE

SPIEDigitalLibrary.org/conference-proceedings-of-spie

Assessment of image quality parameters of a novel micro-CT system compared to a conventional CT geometry

K. Kumar, N. Saeid Nezhad, B H. Mueller, O. Tischenko, C. Hoeschen

K. Kumar, N. Saeid Nezhad, B H. Mueller, O. Tischenko, C. Hoeschen, "Assessment of image quality parameters of a novel micro-CT system compared to a conventional CT geometry," Proc. SPIE 10573, Medical Imaging 2018: Physics of Medical Imaging, 105732L (9 March 2018); doi: 10.1117/12.2293774



Event: SPIE Medical Imaging, 2018, Houston, Texas, United States

Assessment of image quality parameters of a novel micro-CT system compared to a conventional CT geometry

K. Kumar^{1*}, N. Saeid Nezhad^{1*}, B. H. Mueller¹, O. Tischenko², C. Hoeschen¹

¹Otto-von-Guericke University Magdeburg, Institute of Medical Engineering, Magdeburg, Germany

²Helmholtz Center Munich, Neuherberg, Germany

ABSTRACT

A novel fourth generation micro-CT (WATCH-CT) with a unique scanning geometry, that collects parallel projections from a standard x-ray source without the requirement to interpolate or rebin the data, is studied and evaluated for its imaging qualities and performance characteristics. For a comparative analysis of the WATCH micro-CT system and the conventional CT geometry, the local noise power spectrum and the modulation transfer function is derived from the same initial parameters. The spatial resolution (MTF), characterized by the response of the system, is determined by the MTF derived by the oversampling method. The calculations involve varying the parameters like the region of evaluation (ROE) position, FOV magnification, angular sampling, pixel size, filtration and reconstruction algorithm to provide an extensive analogy between these systems. The spatial resolution of the scanning geometries is evaluated and compared. The MTF curves illustrate a higher relative resolving capacity for the WATCH micro-CT compared to the conventional geometries which is due to the characteristics of this unique geometry. The WATCH system exhibits higher resolutions explicitly at the regions away from the center. The NPS curves of WATCH geometry shows higher noise content in comparison to the conventional geometry.

Keywords: Micro-CT, MTF, NPS, Geant4 toolkit, Monte-Carlo simulation

1. INTRODUCTION

Computed tomography based imaging methodologies has a significant importance in the fields of medical imaging and pre-clinical investigations. Micro-CT systems have shown to provide enhanced resolving capabilities to a micrometer scale that can be effectively applied for detecting smaller deformities and tumours. However, there are drawbacks to this technology: radiation exposure increases with miniaturization of detector elements to improve spatial resolution. This has potentially undesirable effects on the organism to be studied.² Higher relative radiation dose may have detrimental impact on the biological subject rendering it to be unusable for further experimental use and additionally, extending these systems to human applications will also have negative impacts.

In previous works of our group,^{1,2} a new micro scanning system capable of functioning at a lower dose level and a faster reconstruction protocol, called as Well Advanced Technique for CT with High Resolution (WATCH), has been proposed that is capable of collecting parallel projections from a standard x-ray source without the requirement to conduct the process of interpolation or re-binning the tomographic projection data. Here a comparison of image quality performance has been conducted between the WATCH and the conventional CT geometry using the orthogonal Polynomial Expansion on Disk (OPED) algorithm and filtered back projection (FBP), respectively on the projection data collected from Monte Carlo simulations.

The resolving capabilities of a digital imaging system can be efficiently determined by the spatial frequency response using the slanted-edge method. The modulation transfer function (MTF) is a basic performance measure of an imaging system describing the signal transfer characteristics of the system as a function of spatial frequency.⁴

Further author information: (Send correspondence to N. Saeid nezhad)

E-mail: nazila.saeid@ovgu.de, Telephone: +493916757271

Medical Imaging 2018: Physics of Medical Imaging, edited by Joseph Y. Lo, Taly Gilat Schmidt, Guang-Hong Chen, Proc. of SPIE Vol. 10573, 105732L © 2018 SPIE · CCC code: 1605-7422/18/\$18 · doi: 10.1117/12.2293774

^{*}The first two authors have equal contribution.

For digital imaging systems with a discrete image sampling a characteristic difficulty arises because the response of the detector to a signal pattern may not only depend on the imaging properties of the detector itself but also on the signal pattern and its location relative to the sampling grid of the detector.⁵ Additionally, the noise spectral densities of the imaging systems are evaluated and compared between the conventional CT geometry and the WATCH system. In diagnostic CT imaging, noise is mainly caused by photon detection statistics⁶ and cannot be avoided due to the desire to limit radiation dose. Noise spectral analysis is capable of providing the noise content information at different spatial frequencies, giving a complete assessment of the imaging quality.

The important aspects of this paper involves the fundamental aim of comparing the novel micro-CT (WATCH) system with the conventional CT geometry to establish effective evidences that support the claimed advantages associated with the WATCH system over the conventional geometry. To provide a fair analogy, the two systems are compared under the effects of the ideal reconstruction algorithm associated with them, i.e. the OPED (Orthogonal Polynomial Expansion on Disk) associated with the WATCH geometry and the FBP with the conventional CT geometry.

2. BACKGROUND

2.1 Scanning Geometry

Formally, a ray $l(\theta, t)$ is a line described by equation:

$$x\cos\theta + y\sin\theta = t$$

In other words:

$$l(\theta, t) : \{(x, y) | x cos\theta + y sin\theta = t\}$$

Angle θ is referred to as a projection angle of the ray, and t is the signed distance between the line and the origin of the coordinate system xy (see left in Fig. 1 for the meaning of parameters).

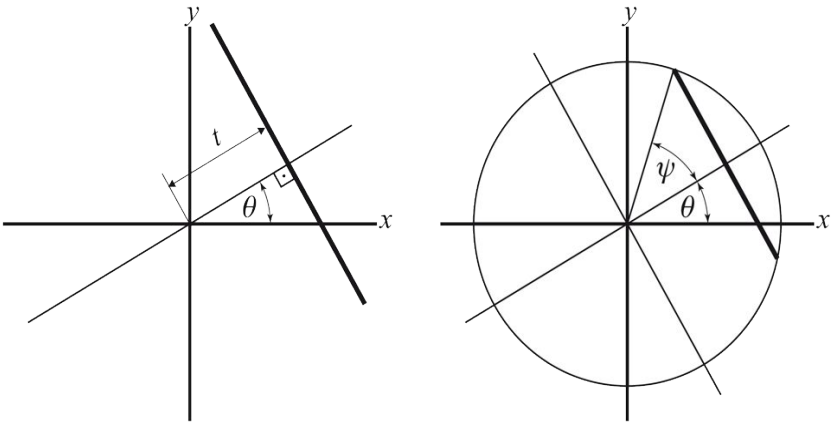


Figure 1: Two equivalent representations of the same ray (fat line).

The same line can equivalently be described by angle parameter ψ (see right in Fig. 1 for the meaning of this parameter). Therefore, the relation:

$$t = \cos \psi$$

is valid.

In tomography one collects data in form of integrals over discrete set of lines. The configuration of the lines is referred to as the data geometry. The data geometry where the set of all lines is represented by the groups of parallel lines is called parallel beam geometry. There are two interesting kinds of parallel beam geometry:

1) parallel lines are described by t_i ,

$$t_j = t_0 + j\frac{R}{M}, j = -M, ..., M$$

2) parallel lines are described by angle parameter ψ_j ,

$$\psi_j = \psi_0 + j\frac{\pi}{M}, j = 0, ..., M - 1$$

Corresponding distributions of rays are depicted in Fig. 2, left and right respectively.

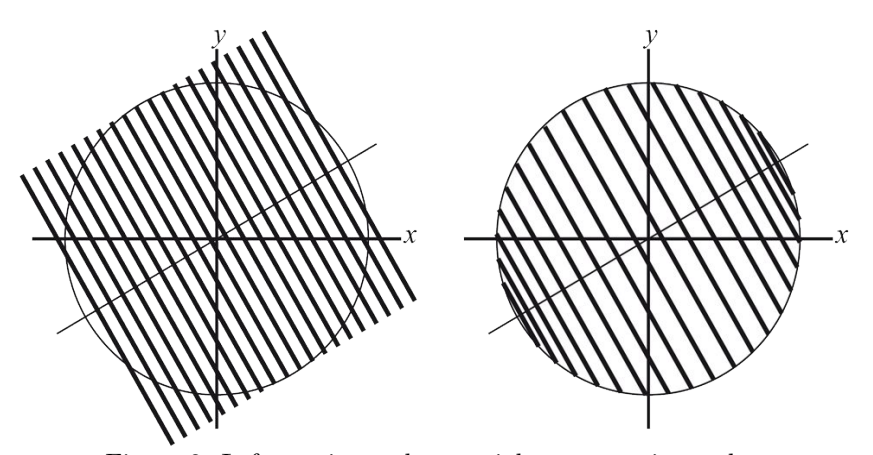


Figure 2: Left: equispaced rays; right: non-equispaced rays

The first kind of parallel data is natural for the reconstruction with FBP-algorithm, while the second kind is natural for the reconstruction with OPED-algorithm.

2.2 OPED Reconstruction Algorithm

The OPED reconstruction algorithm, based on the Orthogonal Polynomial Expansion on the Disc method, is an advanced form of reconstruction technique proposed by O. Tischenko et al.¹ that requires parallel projection data. The OPED algorithm is based on a geometry in which parallel rays are not equally spaced but follow the distribution of the zeros of Chebyshev polynomials of a given order.⁹ One of the specific requirements for the reconstruction algorithm OPED (Orthogonal Polynomial Expansion on Disk) is that Radon projections have to be ψ -projections. This means that fan data can be re-sampled to data required by OPED via some loss-free interpolation. Projections generated by parallel rays intersecting points, which are uniformly distributed on the boundary of disk, represent an example of data which can be re-sampled to fan data and vice versa without loss of information. Projections of such geometry are referred in O. Tischenko et al.¹ to as ψ -projections, and the corresponding parameterization as ψ -parameterization.¹ The algorithm OPED consists of approximating the function f(x, y) that we want to reconstruct as an expansion A_N in N Chebyshev Polynomials U_k of order $k = 0, \ldots, N-1.^9$ The approximation can be given as,

$$A_N f(x,y) = \underbrace{\frac{1}{N}}_{1} \sum_{v=0}^{N-1} \sum_{k=0}^{N-1} \underbrace{(k+1)}_{2} \underbrace{U_k(x cos\phi_v + x sin\phi_v)}_{3} \underbrace{\frac{1}{\pi} \int_{-1}^{1} R_f(\phi_v, t) U_k(t) dt}_{4}$$

Where, the first part (1) is a normalization factor, second (2) are the reciprocals for the frequency. They are a weight for the corresponding components in the expansion. Third part (3) is the corresponding basis vector, i.e. a Chebyshev ridge polynomial of the second kind and the fourth part (4) is the corresponding coefficient of the expansion in those basis vectors, i.e. the scalar product of the Radon data (obtained with the CT-scanner) and the basis vectors. This integral is approximated with a Gaussian quadrature. The OPED algorithm is utilized in this work for reconstruction of the projections from the WATCH geometry that collects parallel data as required by this method.

3. METHODS AND MATERIALS

The projection data was collected from the Monte Carlo simulations of the imaging geometry of the WATCH system and a conventional CT geometry using Geant4 Monte Carlo simulation under identical setup of the geometrical parameters. The WATCH geometry simulations on Geant4 toolkit, are based on the previously proposed scanner system.²

The geometric parameters were established defining similar conditions for the simulation process for the two scanning geometries. The determining parameters include the source object distance (SOD), source detector distance (SDD), Beam opening angle (β) , number of detector elements (N_{pix}) , number of the projections (N_{view}) , the scale of the rectangular detector elements for both dimensions x and y (P_x, P_y) and the Image matrix size (I_{mat}) , as displayed in Tab. 1).

PARAMETER	WATCH-CT	CONVCT
SOD	100mm	100mm
SDD	200mm	200mm
Fan angle	28°	28°
N_{pix}	900	140
N_{view}	1040,2080,3120	1040,2080,3120
P_x	0.7 mm	0.7 mm
P_y	1 mm	1 mm
I_{mat}	512×512	512×512

Table 1: Simulation parameters of the WATCH system and the conventional CT geometry

3.1 Reconstruction Parameters

The images are reconstructed for the both geometries under additional parameters to analyze the effects of these parameters on the respective scanning geometries and provide an in depth analogy between them. The reconstructions were carried out using two field of views (FOV) sizes i.e., 98 mm and 179.2 mm, respectively, for the image matrix size (I_{mat}) of 512×512 . This gave the horizontal and vertical image pixel pitch of 0.70 mm and 0.3828125,respectively, for the two FOV sizes. The conventional CT system data was reconstructed using Fan-Beam and Parallel-Beam Filtered back-projection algorithm with the application of reconstruction kernels like sharp, standard and smooth (as an example see Fig. 3a 3c). The WATCH-CT data was reconstructed using OPED reconstruction algorithm (as an example see Fig. 3b 3d). Moreover, three experiments with 1040, 2080 and 3120 number of the projections were simulated in order to study the influence of angular sampling on the quality of the reconstructed images.

3.2 Modulation Transfer Function and Noise Power Spectrum

The resolving capabilities of the WATCH and the conventional CT have been evaluated with the consideration to reduce all possible factors that may influence the true response of these systems due to the digital sampling characteristics associated with computed tomography. A method of determining the pre-sampled MTF by oversampling edge spread function is applied due to the dependence of the system response on the sampling grid. For the calculations of the pre-sampled MTF, we used a uniform cube phantom, as used in the linearization

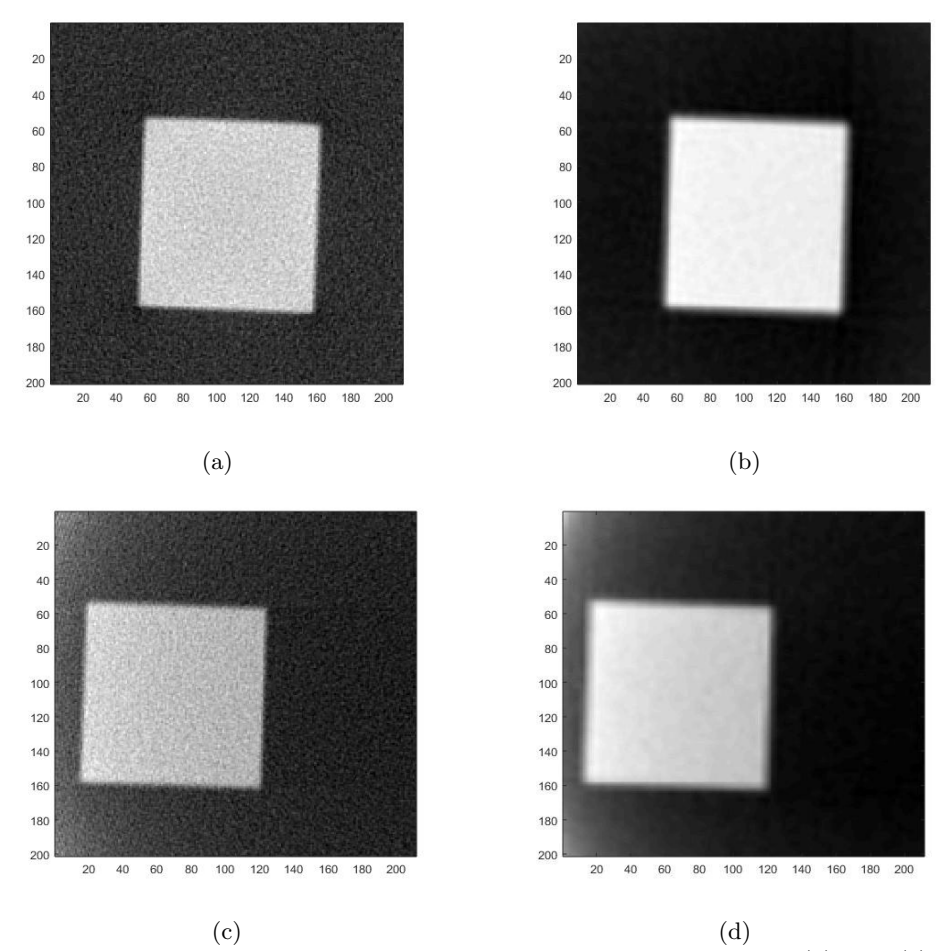


Figure 3: Reconstructed images of the cube used for MTF and NPS estimations. (a) and (c) WATCH images reconstructed by using OPED algorithm for center and off-center positioning of the cube phantom. (b) and (d) conventional CT images reconstructed by using FBP algorithm for center and off-center positioning of the cube object.

process, to utilize its edge properties. The phantom is inclined at an angle of 2° with the consideration of the effects of the relative error Δ MTF/MTF as indicated by E. Buhr et al.,⁵ that show a higher relative error with the increase of edge tilt angle due to decrease in the average number of lines available per edge shift by one pixel. Hence the edge angle is kept within an acceptable range.

The region of interest (ROI) is applied on the reconstructed images for central positions of the FOV as well as for the offset positions. The central and offset ROIs are set at a distance of 10 mm and 64 mm respectively from the center of the FOV. The ROI sizes in terms of pixels are 64 and 117, respectively for the FOV sizes of 98 mm and 179.2 mm. Further steps involve construction of an over-sampled edge spread function from the data points defined by the pixels in the region of interest (ROI). It uses a group of N consecutive lines to construct the over-sampled ESF, where N is determined by the condition that the total shift of the edge transition from the first line to the Nth line should be as close as possible to one pixel in the x direction. The second step of the algorithm is to interlace N consecutive lines to construct the over-sampled edge profile. The third step is to assume as an approximation that the data points belonging to the over-sampled edge profile have been sampled on a regular subsampling grid rather than on the true one. The data set describing the over-sampled line spread function (LSF) is derived from the over-sampled ESF by finite-element differentiation using, e.g., a convolution filter with a [-0.5,0,0.5] kernel.⁵ The MTF is then finally derived by using fast Fourier transform of the edge spread function which is further normalized and corrected.

The noise behaviour assessment using the power spectrum analysis characterizes a stationary behaviour. However, due the variation in the detected X-ray photon counts the method of determining local noise power spectrum is adopted. As per the international standard IEC 62220-1,⁸ the noise power spectrum is determined using the relation,

$$NPS(u_n, v_k) = \frac{\Delta x. \Delta y}{(M.p.q)} \sum_{i=1}^{M} |\sum_{i=1}^{p} \sum_{j=1}^{q} (I(x_i, y_j) - S(x_i, y_j)) exp(-2\pi i (u_n x_i + v_k y_j))|^2$$

Where, Δx and Δy are the pixel spacing in respectively the horizontal and vertical direction, is M the number of regions of interest (ROI)s, $I(x_i, y_j)$ is the linearized data, $S(x_i, y_j)$ is the optionally fitted two-dimensional polynomial, p.q is the size of the ROI. The noise power spectrum is evaluated for the region of interest (ROI) on the reconstructed images for central positions of the FOV as well as for the offset positions. The similar calculation parameters are maintained using the same reconstructed images as used for the evaluation of the modulation transfer function but varying the ROI placement. Evaluation is conducted for both FOV sizes of 98 and 179.2 mm. The size of the region of interest (ROI) is varied as 64×64 and 32×32 array ROI with overlap sizes of 32 and 16 pixels for 64×64 array ROI and 16 pixels for 32×32 array ROI. The two dimensional noise power spectrum is evaluated for all the ROIs individually. As per the international standard IEC 62220-1, seven rows or columns along both sides of the corresponding axis of the two-dimensional NPS, but not the axis itself, are omitted. Two cases are considered prior to the NPS evaluation of the image i.e., in first case the pre-processing steps are applied for DC average removal from the ROI and in the second case no pre-processing is involved. The 2D NPS is averaged for all the ROI to get the noise spectrum which is then used to obtain the one dimensional noise power spectrum along the frequency axis u.

4. RESULTS AND DISCUSSION

The modulation transfer functions are determined for both of the scanning geometries under the calculation parameters setup as discussed in section 3. As a result, Fig. 4, 5 and 6 (left) show a comparative analysis of the resolving capabilities between the WATCH and the conventional CT for the centre position of the cube phantom and for standard, smooth and sharp reconstruction kernels, respectively. Central ROI evaluation exhibits the better resolving capabilities of the WATCH geometry in comparison to the conventional geometry. The MTF curves for the WATCH geometry reconstructed with OPED algorithm has a slightly higher resolution for the central region of the FOV. It is shown that increasing the number of the projections in WATCH system could naturally result in non-equally spaced parallel data with an effect similar to the quarter-detector-shift in conventional CT systems which improves the spatial resolution of the reconstructed images in comparison to the convectional CT scanners where the spatial resolution remains the same, however, in this study, the radiation dose could increase for both systems by increasing the angular sampling. Aliasing artifacts are produced in MTF curves of the conventional CT images which are less visible in MTF curves of the WATCH images reconstructed by OPED algorithm.

The noise characteristics are evaluated as discussed in section 3.2. The noise power spectrum of the uniform ROI with averaging, along with pre-processing, is evaluated for the considered calculation parameters. The Fig. 4, 5 and 6 (right) illustrate the comparison spectrum of the scanning geometries at a region at the center of the FOV for standard, smooth and sharp reconstruction kernels, respectively. The noise level is higher for the images reconstructed from WATCH system in comparison to the conventional CT scanner for 2080 and 3120 angular samples. For 1040 angular samples, the noise magnitude in the WATCH system is fairly similar to the pre-reconstruction magnified images reconstructed with parallel beam FBP algorithm for a conventional CT system. The noise content of the WATCH images can be reduced, but this is outside the scope of our article.

The MTF and NPS have been also compared while the cube object was placed off-center to indicate the WATCH image resolution enhancement particularly at the region away from the center. In either case of the object positioning in the WATCH geometry, the spatial resolution of the WATCH system increases with the increase in the number of angular samples and the noise magnitude is higher for 2080 and 3120 angular samples in comparison to the conventional CT system. The results are shown in Fig. 7, 8 and 9 (left) for MTF assessment

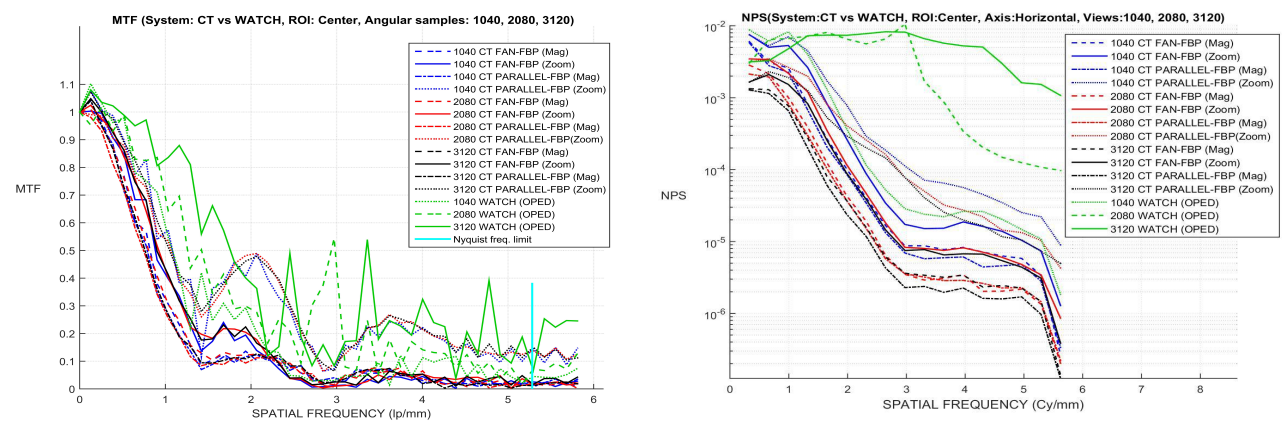


Figure 4: (left) Comparison of the modulation transfer function for the WATCH-CT and the conventional CT geometry for <u>center</u> position of the cube, different number of the views and <u>standard</u> kernel filter, (right) comparison of Noise Spectral density for the WATCH and the conventional CT geometry for <u>center</u> position of the cube, different number of the views and <u>standard</u> kernel filter

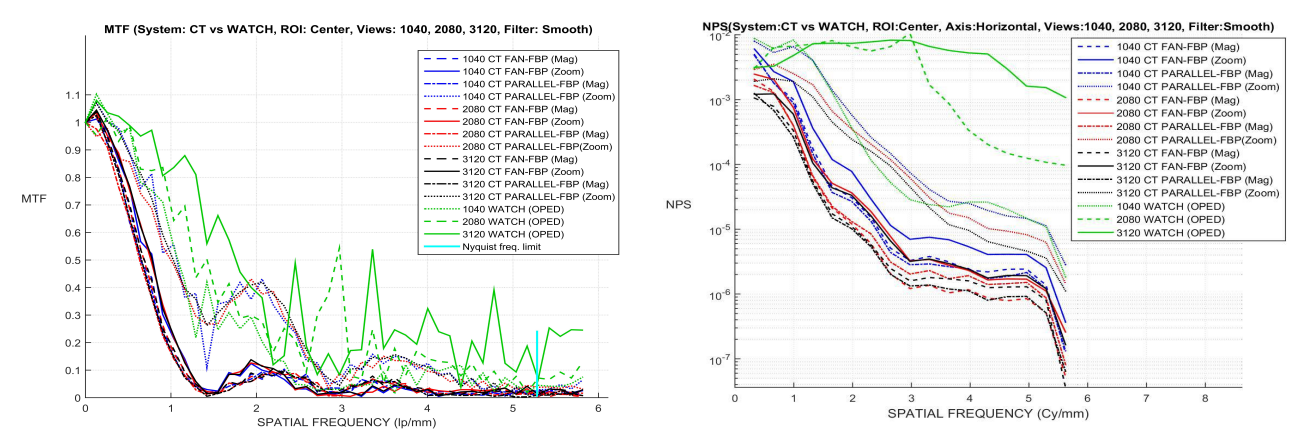


Figure 5: (left) Comparison of the modulation transfer function for the WATCH-CT and the conventional CT geometry for <u>center</u> position of the cube, different number of the views and <u>smooth</u> kernel filter, (right) comparison of Noise Spectral density for the WATCH and the conventional CT geometry for <u>center</u> position of the cube, different number of the views and smooth kernel filter

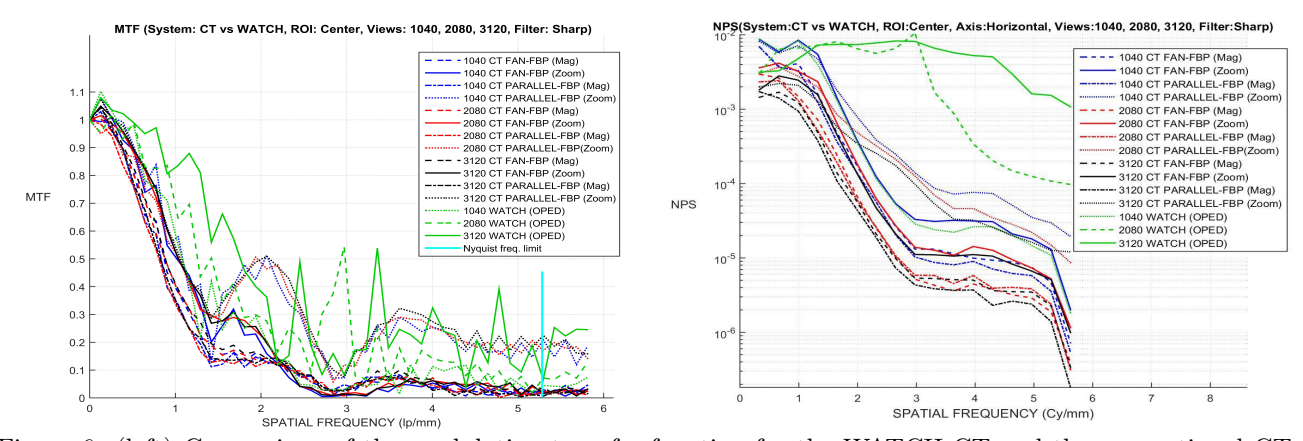


Figure 6: (left) Comparison of the modulation transfer function for the WATCH-CT and the conventional CT geometry for <u>center</u> position of the cube, different number of the views and <u>sharp</u> kernel filter, (right) comparison of Noise Spectral density for the WATCH and the conventional CT geometry for <u>center</u> position of the cube, different number of the views and <u>sharp</u> kernel filter

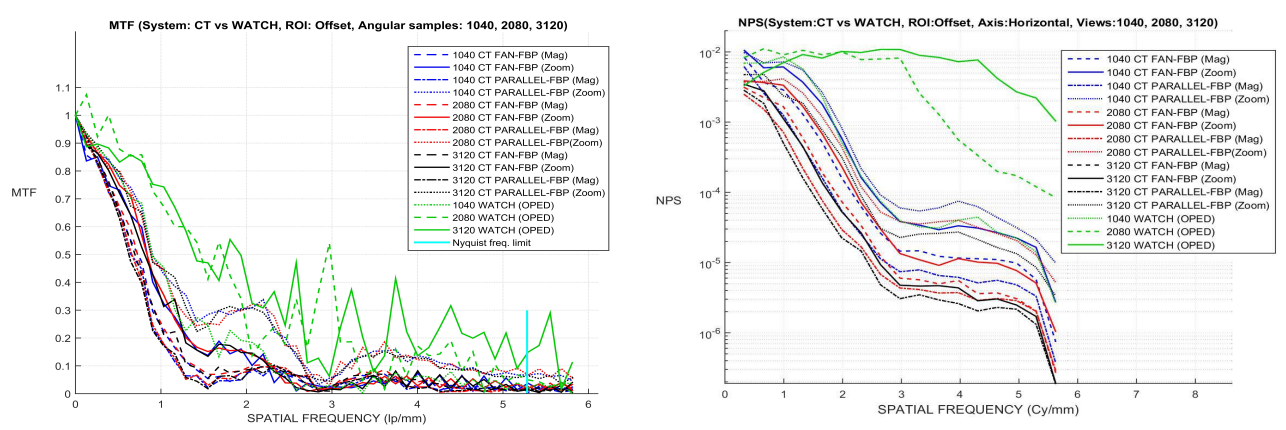


Figure 7: (left) Comparison of the modulation transfer function for the WATCH-CT and the conventional CT geometry for <u>off-center</u> position of the cube, different number of the views and <u>standard</u> kernel filter, (right) comparison of Noise Spectral density for the WATCH and the conventional CT geometry for <u>off-center</u> position of the cube, different number of the projections and <u>standard</u> kernel filter

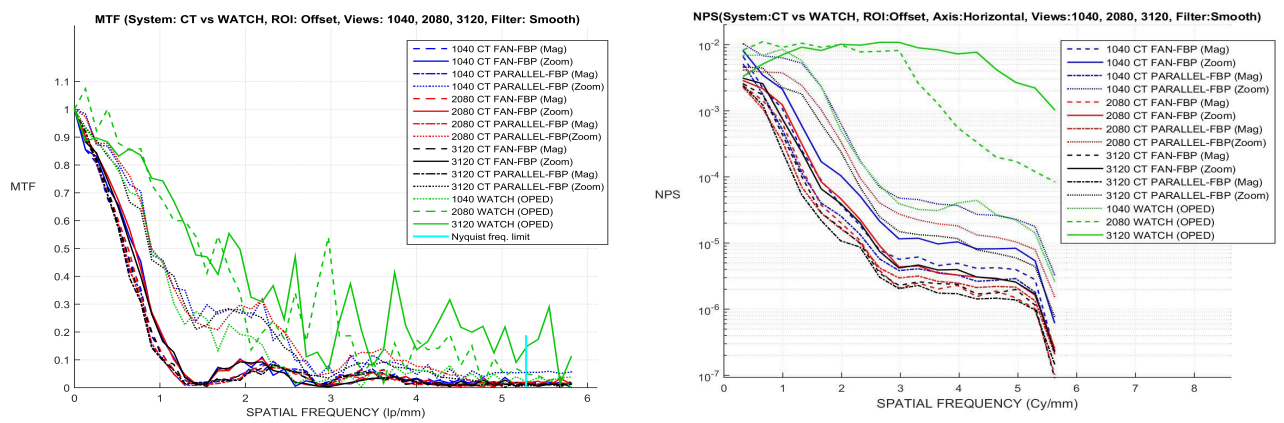


Figure 8: (left) Comparison of the modulation transfer function for the WATCH-CT and the conventional CT geometry for <u>off-center</u> position of the cube, different number of the views and <u>smooth</u> kernel filter, (right) comparison of Noise Spectral density for the WATCH and the conventional CT geometry for <u>off-center</u> position of the cube, different number of the projections and smooth kernel filter

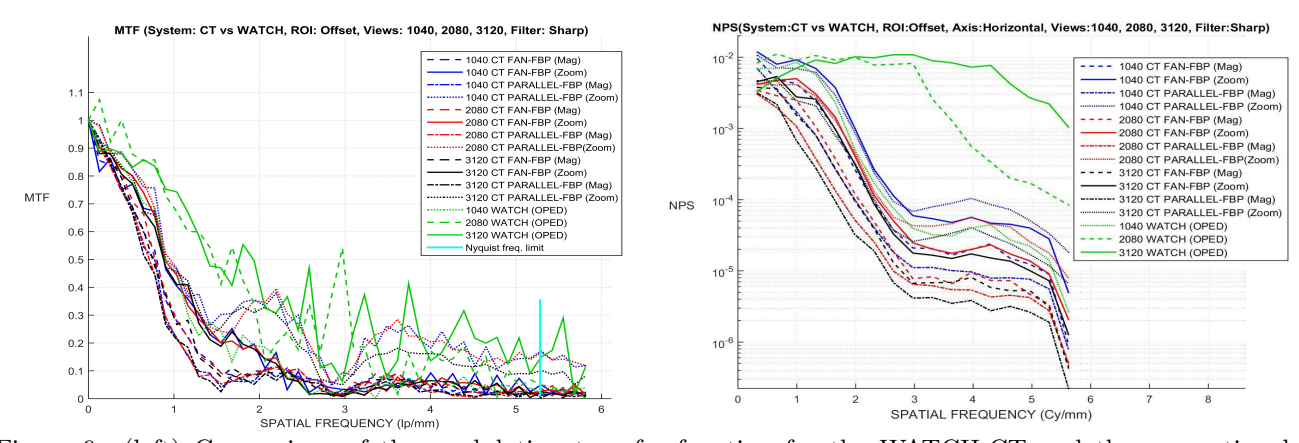


Figure 9: (left) Comparison of the modulation transfer function for the WATCH-CT and the conventional CT geometry for off-center position of the cube, different number of the views and sharp kernel filter, (right) comparison of Noise Spectral density for the WATCH and the conventional CT geometry for off-center position of the cube, different number of the projections and sharp kernel filter

and in Fig. 7, 8 and 9 (right) for NPS measurements for reconstruction of the images with respective reconstruction kernels for FBP algorithm; OPED does not require filtering.³

5. CONCLUSION

In this work, the image quality performance of the WATCH-CT is compared with the conventional CT geometry in depth to determine and analyze the true behaviour of the novel WATCH geometry that collects parallel projections from a standard x-ray source. Through this study, the dependant and independent factors of the WATCH system associated with the OPED are effectively determined through the measurements of the modulation transfer function and the noise power spectrum. The WATCH geometry in combination with OPED reconstruction algorithm exhibits a unique method of imaging in the field of micro-CT which could be effectively extended with the advantages associated with it.

6. ACKNOWLEDGEMENT

We thank Dr. Matthias Greiter and Dr. Hartmut Illers, Helmholtz center in Munich for assistance with MTF and NPS methodology. We would also like to show our gratitude to the Dr. Helmut Schlattl, Helmholtz center in Munich for sharing his pearls of wisdom with us during the course of this research.

REFERENCES

- 1. O. Tischenko, A. Schegerer, Y. Xu, Ch. Hoeschen, Properties of a Parameterization of Radon Projection by the Reconstruction on Circular Disk, Proc. of SPIE Vol. 7622, 2010
- 2. M. Klaften, A. Schegerer, O. Tischenko, M. Hrabe de Angelis, and C. Hoeschen A new design for micro-CT scanner, Spriner, ch. 8, pp. 135-166, 2013
- 3. F. Herold, O. Tischenko, C. Seidl, M. Kurfiss Fast and Analytical Exact Reconstruction of Large CT-Volumes, 18th World conference on Nondestructive Testing, South Africa, 2012
- 4. T.L. Williams The Optical Transfer Function of Imaging Systems, Institute of Physics Publ., Bistrol, 1999.
- 5. E. Buhr, S. Guenther-Kohfahl, U. Neitzel Accuracy of a simple method for deriving the presampled modulation transfer function of a digital radiographic system from an edge image, "Med Phys 2003;30: 2323-31
- 6. R. Loudon The quantum Theory of Light, 3rd ed., Oxford University Press, New York, 2000, p. 117
- 7. J. Baek, NJ. Pelc, the noise power spectrum in CT with direct fan beam reconstruction, Medical physics, 2010; 37(5):2074-2081. doi:10.1118/1.3378673
- 8. International Electronical Commission (IEC), Medical electrical equipment Characteristics of digital X-ray imaging devices, IEC 62220-1:2003 (E), 2003
- 9. Hugo de las Heras. Development and test of a new scanning geometry for Computed Tomography, , Ph.D. Thesis, Helmholtz center of Munich, 2008
- T. M. Buzug Computed Tomography: From Photon Statistics to Modern Cone-Beam CT, Springer, p. 293, 2008